JMEPEG (2013) 22:2073–2079
DOI: 10.1007/s11665-013-0480-8

1059-9495/$19.00

Grain Size Control of the Magnetic Nanoparticles by Solid State Route Modification

A.C.H. Barreto, V.R. Santiago, R.M. Freire, S.E. Mazzetto, J.M. Sasaki, I.F. Vasconcelos, J.C. Denardin, Giuseppe Mele, Luigi Carbone, and P.B.A. Fechine

(Submitted August 20, 2012; in revised form December 5, 2012; published online January 29, 2013)

The $CoFe_2O_4$ and $NiFe_2O_4$ nanoparticles were synthesized exploiting a co-precipitation method and afterward calcinated at 400 °C through two different experimental apparatus: a conventional muffle and rotatory oven. X-ray diffraction (XRD) analysis revealed that nanocrystalline ferrites grew with a face center cubic structure (fcc) and *Fd3m* symmetry space group. XRD, transmission electron microscopy, and magnetic measurements confirmed the compositional homogeneity and the narrow size particle distribution (6-8 nm) of the sample thermally treated in a rotary oven, in all likelihood due to the sample's constant turning movement. The size of the magnetic particles is extremely important and influences the choice of a potential technological application. For this reason, our study emerges as a new and simple innovating procedure to control the size of magnetic nanoparticles.

Keywords $CoFe_2O_4$, magnetic nanoparticles, $NiFe_2O_4$, size grain control

1. Introduction

Spinel ferrite nanoparticles constitute an important class of magnetic ceramics owing magnetic and electrical properties depending on the nature and distribution of their cations in the tetrahedral and octahedral sub-lattices cubic structure (Ref 1). These magnetic nanoparticles have attracted enormous interest as agents for biomedical applications in the fields of magnetic resonance imaging (MRI), magnetic separation, targeted drug delivery, tissue engineering, cell tracking, bioseparation, and magnetic hyperthermia (Ref 2, 3).

A.C.H. Barreto and **V.R. Santiago**, Grupo de Química de Materiais Avançados (GQMAT), Departamento de Química Analítica e Físico-Química, Universidade Federal do Ceará – UFC, Campus do Pici, CP 12100, Fortaleza, CE CEP 60451-970, Brazil; and Laboratório de Produtos e Tecnologia em Processos – LPT, Departamento de Química Orgânica e Inorgânica, Universidade Federal do Ceará, Fortaleza, CE, Brazil; **R.M. Freire** and **P.B.A. Fechine**, Grupo de Química de Materiais Avançados (GQMAT), Departamento de Química Analítica e Físico-Química, Universidade Federal do Ceará – UFC, Campus do Pici, CP 12100, Fortaleza, CE CEP 60451-970, Brazil; **S.E. Mazzetto**, Laboratório de Produtos e Tecnologia em Processos – LPT, Departamento de Química Orgânica e Inorgânica, Universidade Federal do Ceará, Fortaleza, CE, Brazil; **J.M. Sasaki**, Laboratório de Raios X, Departamento de Física, Universidade Federal do Ceará, Campus do Pici, Fortaleza, CE, Brazil; **I.F. Vasconcelos**, Departamento de Engenharia Metalúrgica e de Materiais, Universidade Federal do Ceará, Fortaleza, CE, Brazil; **J.C. Denardin**, Departamento de Física, Universidad de Santiago de Chile, USACH, Av. Ecuador 3493, Santiago, Chile; **Giuseppe Mele**, Dipartimento di Ingegneria dell'Innovazione, Università del Salento, Via Arnesano, 73100 Lecce, Italy; and **Luigi Carbone**, Istituto Nanoscienze UOS Lecce – NNL, Via Arnesano 16, 73100 Lecce, Italy. Contact e-mail: fechine@ufc.br.

In the last few years, several synthetic routes to achieve magnetic nanoparticles have been reported and intensively investigated, as for instance a sonochemical procedure (Ref 4), sol-gel pyrolysis method (Ref 5), hydrothermal technique (Ref 6), and mechanical alloying (Ref 7). However, as it is well known, co-precipitation is a chemical-physics technique that is mostly used and it is an economical way in the production of spinel ferrites nanoparticles due to its simplicity and efficient chemical pathway for the preparation of various interesting solid-state materials (Ref 7, 8). Spinel ferrites have the general molecular formula $(A^{2+})\ (B^{3+})_2(O^{2-})_4$ where divalent and trivalent cations A and B occupy, respectively, the tetrahedral and octahedral interstitial positions of the fcc crystal lattice formed by O^{2-} ions (Ref 9).

Shen et al. (Ref 10) investigated the applicability of magnetic nanoparticles for treating wastewater contaminated by toxic heavy metals. They observed that adsorption capacity of Fe_3O_4 nanoparticles increased with decreasing the particle size. The colloidal magnetic particles dispersed in a magnetic fluid are usually composed of iron, nickel, cobalt, iron oxides, and various ferrites. The stability of magnetic fluids is also mainly dependent on the size of the particle (Ref 11). In the field of medical applications, particles with sizes in the 10-100 nm range are optimal for in vivo long circulation times, whereas particles smaller than 10 nm are rapidly removed by the renal clearance process (Ref 12). Thus, in such applications, an improved control of the magnetic nanoparticle size becomes vital.

In this work, we report on the structure and magnetic properties of $CoFe_2O_4$ and $NiFe_2O_4$ nanoparticles synthesized by co-precipitation and calcinated through two different thermal methods: specifically, using either a conventional muffle or a rotary oven. Thereafter, we focused on the composition homogeneity and size grain control obtained from the two above-mentioned synthesis routes. The nanoparticles size, structure, and composition were characterized by x-ray diffraction (XRD), ^{57}Fe Mössbauer spectroscopy, transmission electron microscopy (TEM), and magnetic measurements.

2. Experimental

2.1 Materials

All reagents were commercial products of analytical grade without further purification. The chemical reagents for this work are $FeCl_3{\cdot}6H_2O$ (Vetec), $CoCl_2{\cdot}6H_2O$ (Dinâmica), $NiCl_2{\cdot}6H_2O$ (Vetec), and 30% ammonia solution (Synth).

2.2 Synthesis of Magnetic Nanoparticles

In the co-precipitation processing route, the solutions of metallic salts either containing Co^{2+} and Fe^{3+} or Ni^{2+} and Fe^{3+} were dissolved and mixed in milli-Q water in the 1:2 molar ratio to form $CoFe_2O_4$ and $NiFe_2O_4$ ferrite phases, respectively. The aqueous mixtures were heated at 80 °C and then added into a 30 wt.% NH_4OH solution at pH 10 to form a black precipitate. The diverse precipitates were repeatedly rinsed with milli-Q water until the residual solution became neutral. Finally, the nanoparticles were dried in a desiccator, then the powder divided in two parts for calcination, both in the rotary oven (Fig. 1) and the muffle oven (sample stationary during experiment), carried out for 1 h at 400 °C under air atmosphere. The reactions occurring during calcination can be summarized as follows:

$$Co^{2+} + 2Fe^{3+} + 8OH^- \rightarrow CoFe_2O_4 + 4H_2O, \quad \text{(Eq 1)}$$

$$Ni^{2+} + 2Fe^{3+} + 8OH^- \rightarrow NiFe_2O_4 + 4H_2O. \quad \text{(Eq 2)}$$

In the rotary oven, the sample was mechanically agitated during calcinations. The rotation speed used in our experiments was 100 rpm. This velocity was chosen after some experiments. Figure 1 schematically describes the apparatus; particularly, the oven consists of an engine (component 1) which rotates a 30-cm-length alumina tube (component 2), an oven (step 3) where the alumina tube with the sample is inserted (step 4), and a termopar for regulating and controlling the calcination temperatures (component 5).

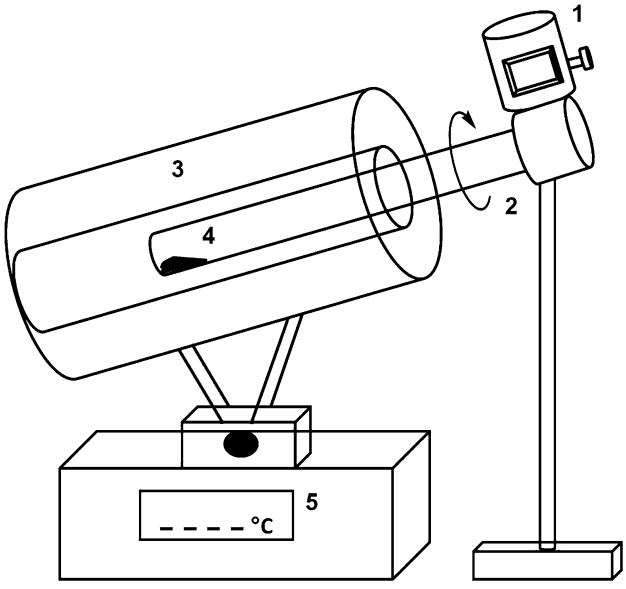

Fig. 1 Rotatory oven

2.3 Characterization

The XRD analysis was performed in a x-ray powder diffractometer Xpert Pro MPD (Panalytical) using Bragg-Brentano geometry in the range of 20-120° with a rate of 1°/min. Co-K_α radiation (λ = 1.7889 Å) was used and the tube operated at 40 KV and 30 mA. The phase identification analysis was made by comparing powder diffractograms with standard patterns from the International Centre for Diffraction Data (ICDD). Rietveld refinement procedures (Ref 13, 14) were applied to all diffraction patterns using the DBWS 2.25, as described by Young and coworkers (Ref 13, 15). The peak full width at half maximum (FWHM) resulting from refinement was used to calculate the nanoparticle size for {111}, {220}, {311}, {400}, {422}, {511}, {440}, {533}, and {553} crystallographic families. The ferrite average core size can be obtained using the well-known Scherrer's equation:

$$D = \frac{K\lambda}{\beta \cos\theta}, \quad \text{(Eq 3)}$$

where D represents the average particle diameter, K is the Scherrer constant, λ is the x-ray wavelength, β is the peak FWHM, and θ is the Bragg's angle in degree. The β parameter was corrected for the instrumental broadening using the following equation:

$$\beta = \sqrt{\beta_{exp}^2 - \beta_{inst}^2}, \quad \text{(Eq 4)}$$

where β_{exp} is the measured broadening and β_{inst} is the broadening due to the instrument. β_{inst} was obtained from the standard LaB_6 powder (SRM 660-National Institute of Standard Technology) using the Caglioti's equation (Ref 13, 16):

$$\beta_{inst} = \sqrt{U\tan^2\theta + V\tan\theta + W}, \quad \text{(Eq 5)}$$

where U, V, and W were obtained from the Rietveld refinement analysis. In the model proposed by Williamsom-Hall (Ref 13, 17), the particle size (D) and microstrain (ε) are convoluted in the integral breadth of the peak profile and both parameters can be analytically separated by means of the following equation:

$$\beta\cos\theta = \frac{\lambda}{D} + 4\varepsilon\sin\theta, \quad \text{(Eq 6)}$$

where λ is the wavelength of incident radiation. The plotting $\beta\cos\theta/\lambda$ versus $\sin\theta$ gives the particle size from the linear and angular coefficients of the straight line obtained.

The magnetization measurements were performed at room temperature with a homemade vibrating sample magnetometer (VSM). The VSM has been previously calibrated using a pure Ni wire, and after measuring the mass of each sample, the magnetization was given in emu/g.

^{57}Fe Mössbauer spectra were acquired using standard transmission geometry and a constant acceleration spectrometer, with a radioactive source of ^{57}Co in Rh matrix. Measurements were carried out at laboratory temperature (about 294 K) on powder samples with an absorber thickness of 2 mg/cm^2. Theoretic fits using a minimum number of Lorentzian spectral components were performed with the fitting software NORMOS written by R.A. Brand (distributed by Wissenschaftliche Elektronik GmbH, Germany). The spectrum consists of a set of magnetic subspectra related to the $CoFe_2O_4$ and $NiFe_2O_4$

nanoparticles' structure. All the isomer shifts (δ) quoted in this paper are relative to metallic iron (α-Fe).

Low-magnification TEM analysis is performed on a Jeol JEM-1011 electron microscope operating at 100 kV, equipped with a CCD camera ORIUS 831 from Gatan. TEM samples are prepared by drop casting dilute nanocrystal solutions onto carbon-coated copper grids. Afterward, the deposited samples are allowed to completely dry at 60 °C for one night before examination.

3. Results and Discussion

Figure 2 shows x-ray powder diffraction patterns of $NiFe_2O_4$ nanoparticles calcinated by a conventional muffle (a) and rotary oven (b). The gray lines represent the relative difference between the experimental (Y^{Obs}) and the calculated (Y^{Calc}) intensities obtained by the Rietveld refinement. The results indicated that the identified phase is face-centered cubic (JCPDS Card No. 08-4101) with symmetry spatial group *Fd*3*m*. The samples heat treated in the muffle furnace showed the presence of Fe_2O_3 impurity (3.16% in mass) in all likelihood due to an incomplete formation of the ferrite phase during the calcination process. Shi et al. (Ref 8) reported that after annealing at 400 °C, indicating the partial formation of nickel ferrite phase and the complete formation requires heat at 1100 °C or a higher temperature. In order to infer the crystallite's homogeneity, particle sizes were calculated for

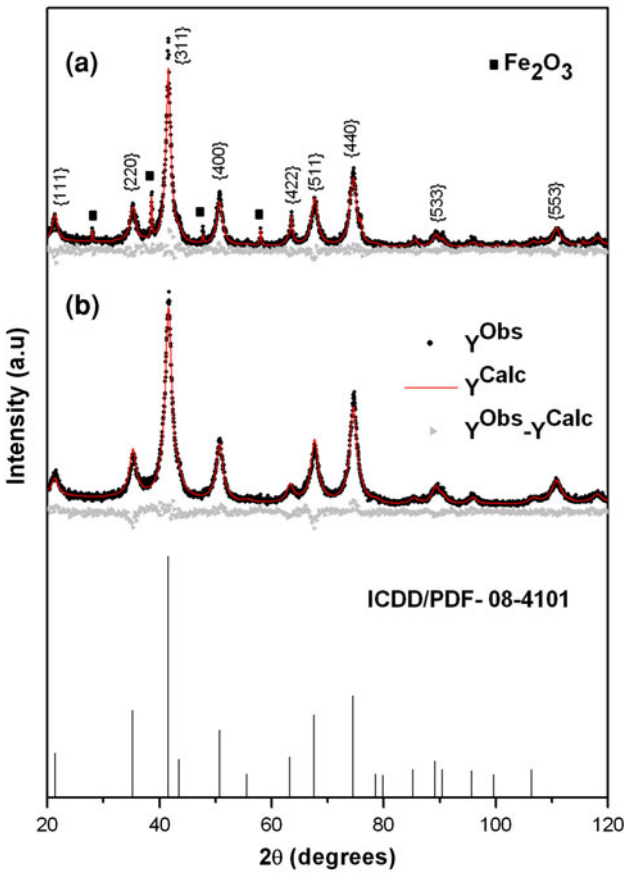

Fig. 2 XRD patterns of $NiFe_2O_4$ nanoparticles calcined in the muffle (a) and rotary oven (b)

nine crystallographic families using Scherrer's equation (3) for all samples as shown in Table 1. It can be noticed that the average particle diameter obtained by the rotary oven (7.5 nm) is smaller compared with nanoparticles annealed in the muffle furnace (8.7 nm). The microstrain obtained by the Williamsom-Hall plotting is also summarized in Table 1. $NiFe_2O_4$ nanoparticles from the rotary oven presented a value of 0.09% for microstrain, while the muffle oven was 0.19%. These results confirm that the annealing process in the rotary oven favors the additional homogeneity in the samples and consequently a smaller grain size. This happened due to the better distribution of the particles' powder into the oven.

X-ray powder diffraction patterns of the $CoFe_2O_4$ nanoparticles treated inside the muffle and rotary oven are presented in Fig. 3(a) and (b), respectively. Both are similar and no impurities from synthesis route were identified. The average grain size was about 7.4 nm for samples processed inside the muffle and 6.4 nm for the rotary oven. Zhao and Jiang (Ref 18) synthesized 30 nm $CoFe_2O_4$ ferrite particles employing an emulsion method. The results also indicated that the identified phase is face-centered cubic (JCPDS Card No. 09-8553) with symmetry spatial group *Fd*3*m*. The minimum microstrain was also reported for samples calcinated in the rotary oven (0.47%) and the muffle oven (0.63%). Thus, relative to both particle systems ($NiFe_2O_4$ and $CoFe_2O_4$), experimental data indicate that the continual sample turning movement produced inside a rotary oven seems to enhance the specimen homogeneity and reduce the particle size.

The morphologies of $NiFe_2O_4$ and $CoFe_2O_4$ nanoparticles from the rotary oven were also investigated by TEM, as shown in Fig. 4. The nanoparticles maintain a roughly spherical shape; furthermore, for a few isolated particles, the size approximated by TEM is consistent with the crystallite sizes of nanoparticles estimated by the Scherrer equation (3). They are polydisperse and most of them agglomerated due to interparticle magneto-dipole interactions. This experimental tendency has been observed in other studies (Ref 18-23).

We have furthermore examined ^{57}Fe Mössbauer spectra of nanoparticles from the muffle oven- and rotary oven-calcinated in order to study the sample's superparamagnetic nature as well as the existence of the Fe in different neighbors. In the Fig. 5, the Mössbauer spectra for $NiFe_2O_4$ consist of two subspectra,

Table 1 Average crystallite sizes and microstrain obtained by x-ray of the $NiFe_2O_4$ and $CoFe_2O_4$ nanoparticles calcined by the conventional muffle and rotary oven

	$CoFe_2O_4$ particle size (nm)		$NiFe_2O_4$ particle size (nm)	
Diffraction plane (hkl)	Muffle oven	Rotary oven	Muffle oven	Rotary oven
111	9.6	7.2	8.6	6.7
220	8.9	7.1	8.9	7.2
311	8.5	7.0	9.0	7.4
400	7.9	6.7	9.1	7.7
422	7.2	6.4	9.0	8.0
511	7.0	6.3	8.9	8.0
440	6.6	6.1	8.8	8.0
533	6.0	5.7	8.4	7.8
553	5.4	5.2	7.7	7.1
Average	7.4 (±0.4)	6.4 (±0.2)	8.7 (±0.1)	7.5 (±0.1)
Microstrain, %	0.63	0.47	0.19	0.09

indicating the presence of Fe atoms with different neighbors. The doublet at the center of the spectra can be attributed to the superparamagnetic relaxation phenomenon due to a small size with particles less than 10 nm (Ref 24), as effectively observed by the XRD (see Fig. 2a). The sextet patterns shown for $NiFe_2O_4$ as prepared by the muffle oven (Fig. 5a) and the rotatory oven (Fig. 5b) were observed to correspond to Fe^{3+} in the spinel structure and another site characteristic of the Fe_2O_3 impurity identified through XRD (see Fig. 2a), respectively. These results clearly pointed to the contribution of the heat type over the calcination process at the purity of the samples.

In these samples, all the spectra were initially adjusted using two magnetic sextets referring to an octahedral site and a tetrahedral site, and it was observed that these sites were indistinguishable. $NiFe_2O_4$ prepared by the muffle oven showed an isomer shift relative to αFe $\delta = 0.37$ mm/s (Sextet) and $\delta = 0.31$ mm/s (Dublet), quadrupole shift $\varepsilon = -0.20$ mm/s (Sextet) and $\delta = -0.68$ mm/s (Dublet), and magnetic hyperfine

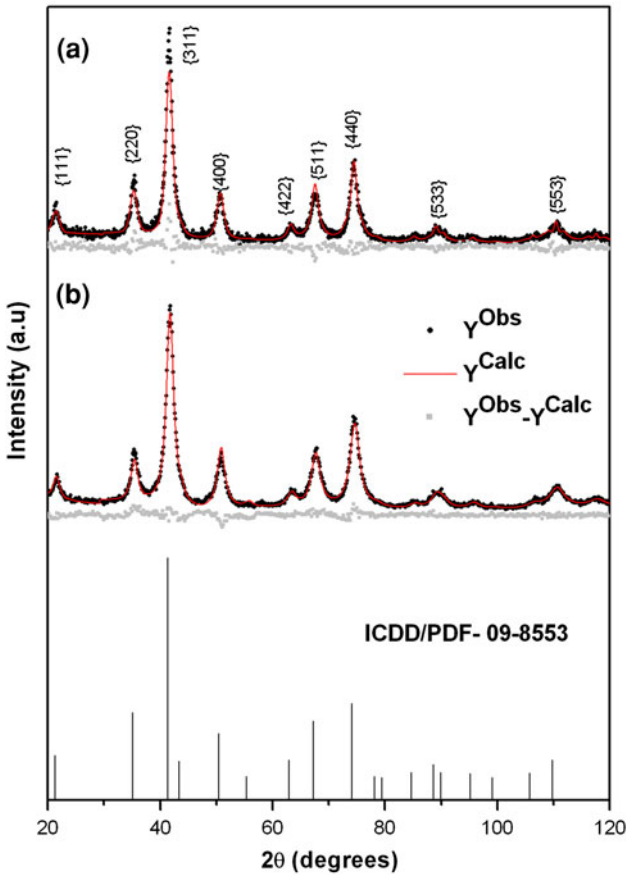

Fig. 3 XRD patterns of $CoFe_2O_4$ nanoparticles calcined in the muffle (a) and rotary oven (b)

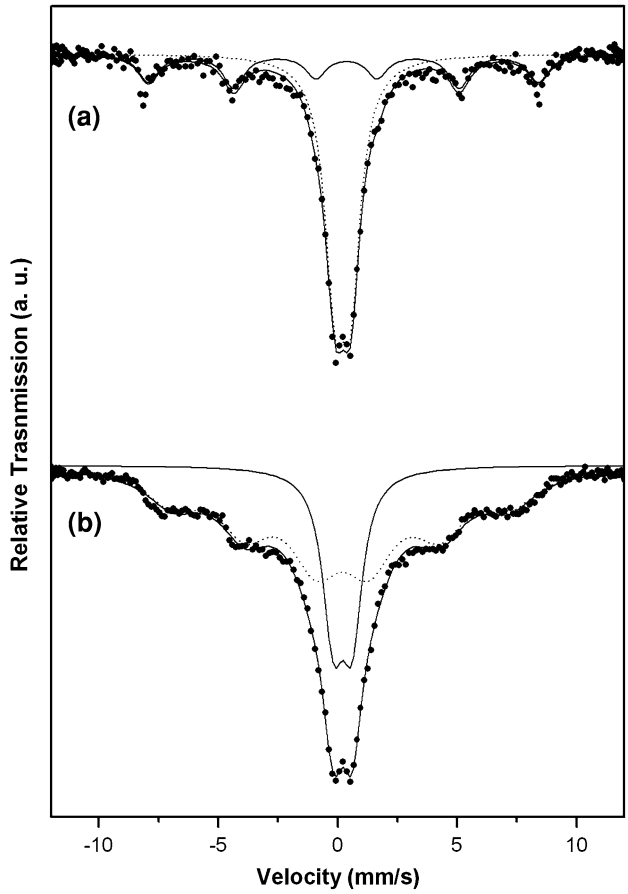

Fig. 5 Mössbauer spectra relative to $NiFe_2O_4$ calcined by the muffle oven (a) and rotary oven (b)

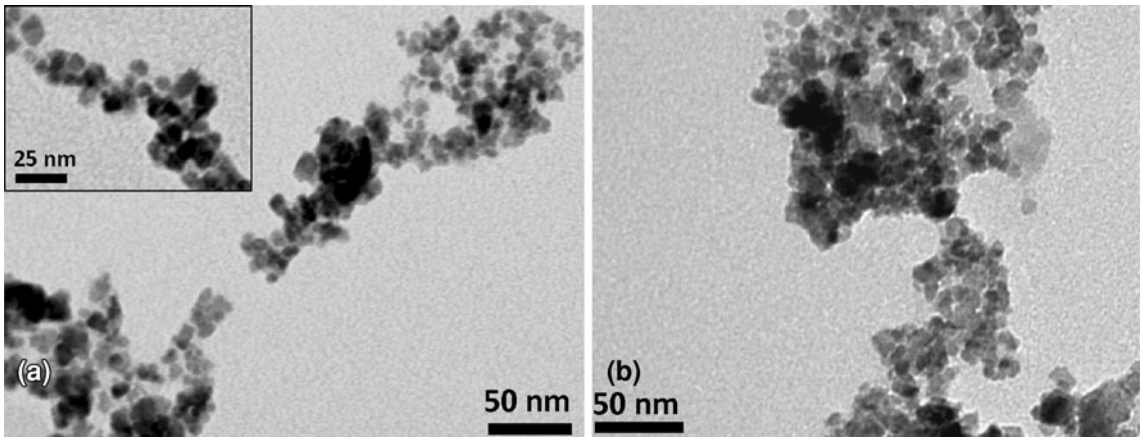

Fig. 4 Low magnification TEM images of (a) $NiFe_2O_4$ and (b) $CoFe_2O_4$ nanoparticles

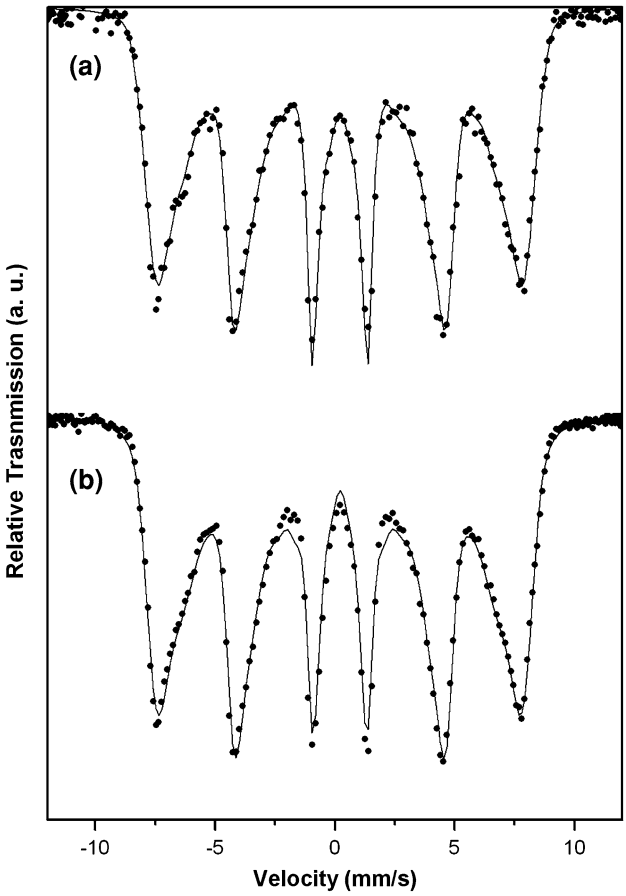

Fig. 6 Mössbauer spectra relative to $CoFe_2O_4$ calcined by the muffle oven (a) and rotary oven (b)

Table 2 Hyperfine parameters for $NiFe_2O_4$ and $CoFe_2O_4$ nanoparticles calcined by the muffle and rotary oven

	$CoFe_2O_4$		$NiFe_2O_4$	
Hyperfine parameters	**Muffle oven**	**Rotary oven**	**Muffle oven**	**Rotary oven**
δ, mm/s	0.32	0.31	0.37[a]/0.31[b]	0.26[a]/0.31[b]
Δ, mm/s	0.0	−0.01	−0.20[a]/−0.68[b]	−0.05[a]/−0.78[b]
B_{HF}, T	48	47.0	51.0	44.0

[a] Sextet/[b] Doublet

field $B_{hf} = 51$ T assignable to hematite, while $NiFe_2O_4$ prepared by the rotary oven showed an isomer shift relative to αFe δ = 0.26 mm/s (Sextet) and δ = 0.31 mm/s (Dublet), quadrupole shift ε = −0.05 mm/s (Sextet) and δ = −0.78 mm/s (Dublet), and magnetic hyperfine field $B_{hf} = 44$ T due to nickel ferrite, according to typical values for this nanoparticle (Ref 25).

On the contrary, $CoFe_2O_4$ Mössbauer spectra did not display significative changes between the muffle oven- and rotary oven-calcinated samples (Fig. 6a and b). The sextet peak observed is mainly due to the ferromagnetic behavior of the nanoparticles. Table 2 summarizes the hyperfine parameters of the nickel and cobalt nanoparticles.

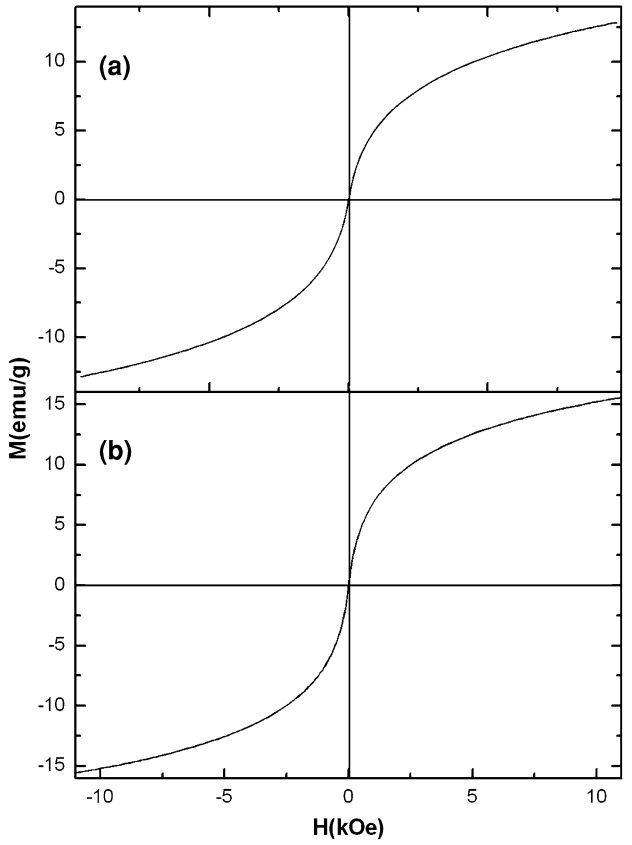

Fig. 7 Hysteresis loops of $NiFe_2O_4$ calcined by the muffle oven (a) and rotary oven (b)

The isomer shifts at room temperature for $CoFe_2O_4$ calcined in the muffle oven were found to be 0.32 mm/s, and for $CoFe_2O_4$ calcined in the rotary oven were 0.31 mm/s. This is characteristic of Fe^{3+} with the high-spin state since according to the literature (Ref 26), values in the range 0.1-0.5 can be attributed to Fe^{3+} in this state. The quadrupole interaction (ε) showed values between −0.78 and 0.68. The relatively high values observed indicate a chemical disorder and a local symmetry reduction in the site. This parameter can be affected by nonspherical charge distribution at the nucleus. This explained the change of the signal observed for the samples because when the nucleus is elongated or flattened, the values of ε remained positive or negative, respectively (Ref 27). Magnetic hyperfine field $B_{hf} = 48$ T for the sample calcined in the muffle oven and 47 T for the sample calcined in the rotary oven.

Figure 7 shows the typical magnetic hysteresis loops for $NiFe_2O_4$ nanoparticles calcinated inside the muffle (Fig. 7a) and rotary oven (Fig. 7b). Vibrating sample magnetometry indicated a different magnetic behavior according to material crystallinity (Ref 28). The hysteresis curves show larger saturation magnetization (M_s) for the rotary oven-calcinated nickel ferrites (15.09 emu/g), when compared to the muffle-treated (12.87 emu/g) ones, see Table 3. These results are mainly ascribed to the presence of Fe_2O_3 impurity as already proved by x-ray analysis and Mössbauer spectra. Basically, the impurity decreases the saturation magnetization of those materials. Laokul et al. (Ref 5) also verified that α-Fe_2O_3 reduces the magnetic properties of ferrites.

Table 3 Magnetic properties of $NiFe_2O_4$ and $CoFe_2O_4$ nanoparticles calcined by the muffle oven and rotary oven

	$CoFe_2O_4$		$NiFe_2O_4$	
Magnetic properties	**Muffle oven**	**Rotary oven**	**Muffle oven**	**Rotary oven**
M_s, emu/g	30.96	29.46	12.87	15.09
M_r, emu/g	5.03	3.47	…	…
H_c, kOe	0.379	0.1926	…	…

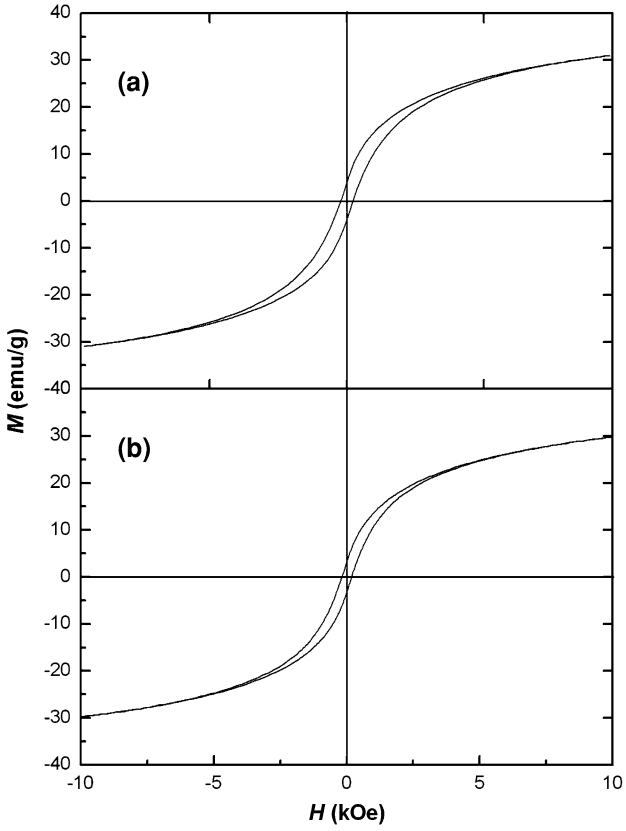

Fig. 8 Hysteresis loops of $CoFe_2O_4$ calcined by the muffle oven (a) and rotary oven (b)

The magnetization behavior of nickel ferrite can be understood in terms of cation distribution and Neel's model (Ref 29). $NiFe_2O_4$ with an inverse spinel structure shows features typical of superparamagnetic materials, mainly due to particle size distribution relative to the two calcination routes. Due to this behavior, it was not possible to observe the coercive field (H_c) and remnant magnetization (M_r) for the samples calcined by both ways.

Similarly, Fig. 8(a) and (b) shows the hysteresis loops of the muffle oven- and rotary oven-calcinated $CoFe_2O_4$ ferrites, respectively. The M_s, H_c, and M_r values for the muffle-treated samples are 30.96 emu/g, 0.379 kOe, and 5.03 emu/g, respectively, whereas data relative to the rotary oven-annealed samples are 29.46 emu/g, 0.1926 kOe, and 3.47 emu/g. The differences observed could be attributed to surface effects stimulated by the distortion of magnetic moments at the surface of the nanocrystallite calcinated in the two different routes (Ref 7). The magnetic parameters derived from the hysteresis loops are detailed in Table 3.

4. Conclusions

$NiFe_2O_4$ and $CoFe_2O_4$ nanoparticles were obtained by the classical co-precipitation synthesis method. While from one side this technique is the most straightforward and efficient to obtain magnetic particles, from another side, it involves a further specimen calcination treatment in order to achieve determined magnetic phases. As thermal experimental equipment, we employed both a conventional muffle and a new designed rotary oven operating at 400 °C for 1 h in order to evaluate the different annealing effects on particle features. We observed that in the case of both $NiFe_2O_4$ and $CoFe_2O_4$, the regular circular sample movement produced by the rotary oven affected the sample compositional homogeneity and decreased the particle size. Mössbauer spectra revealed that $NiFe_2O_4$ nanoparticles thermally treated in the rotary oven are superparamagnetic, whereas nickel ferrites calcinated in the muffle oven showed the presence of Fe_2O_3 impurity, which was proved by XRD. All the observed structural and magnetic properties are in perfect agreement with those reported in the literature, confirming the success of our route of calcinations. Therefore, we recommend our thermal procedure as an accessible methodology for the fabrication of many other nanoparticles in order to control composition and size distribution.

Acknowledgments

The support from CAPES, Funcap, and CNPq (Brazilian agencies); Fondecyt 1110252; Millennium Science Nucleus, Basic and Applied Magnetism Grant No. P10-061-F; and CONICYT BASAL CEDENNA FB0807 (Chilean agencies) is gratefully acknowledged.

References

1. L. Bem Tahar, M. Artus, S. Ammar, L.S. Smiri, F. Herbst, M.J. Vaulay, V. Richard, J.M. Grenèche, F. Villain, and F. Fiévet, Magnetic Properties of $CoFe_{1.9}RE_{0.1}O_4$ Nanoparticles (RE = La, Ce, Nd, Sm, Eu, Gd, Tb, Ho) Prepared in Polyol, *J. Magn. Magn. Mater.*, 2008, **320**, p 3242–3250
2. J. Giri, P. Pradhan, V. Somani, H. Chelawat, S. Chhatre, R. Banerjee, and D. Bahadur, Synthesis and Characterizations of Water-Based Ferrofluids of Substituted Ferrites [$Fe_{1-x}B_xFe_2O_4$, B = Mn, Co (x = 0-1)] for Biomedical Applications, *J. Magn. Magn. Mater.*, 2008, **320**, p 724–730
3. V.I. Shubayev, T.R. Pisanic, II, and S. Jin, Magnetic Nanoparticles for Theragnostics, *Adv. Drug Deliv. Rev.*, 2009, **61**, p 467–477
4. E.H. Kim, H.S. Lee, B.K. Kwak, and B.K. Kim, Synthesis of Ferrofluid with Magnetic Nanoparticles by Sonochemical Method for MRI, Contrast Agent, *J. Magn. Magn. Mater.*, 2005, **289**, p 328–330
5. P. Laokul, V. Amornkitbamrung, S. Seraphin, and S. Maensiri, Characterization and Magnetic Properties of Nanocrystalline $CuFe_2O_4$, $NiFe_2O_4$, $ZnFe_2O_4$ Powders Prepared by the Aloe Vera Extract Solution, *Curr. Appl. Phys.*, 2011, **11**, p 101–108
6. L.J. Cote, A.S. Teja, A.P. Wilkinson, and Z.J. Zhang, Continuous Hydrothermal Synthesis of $CoFe_2O_4$ Nanoparticles, *Fluid Phase Equilib.*, 2003, **210**, p 307–317
7. S.B. Waje, M. Hashim, W.D.W. Yusoff, and Z. Abbas, X-Ray Diffraction Studies on Crystallite of $CoFe_2O_4$ Nanoparticles Prepared Using Mechanical Alloying and Sintering, *Appl. Surf. Sci.*, 2010, **256**, p 3122–3127
8. Y. Shi, J. Ding, and L.J. Wang, $NiFe_2O_4$ Ultrafine Particles Prepared by Co-Precipitation/Mechanical Alloying, *J. Magn. Magn. Mater.*, 1999, **205**, p 249–254

9. C.N. Chinnasamy, A. Narayanasamy, N. Ponpandian, K. Chattopadhyay, K. Shinoda, B. Jeyadevan, K. Tohji, K. Nakatsuka, T. Furubayashi, and I. Nakatani, Mixed Spinel Structure in Nanocrystalline $NiFe_2O_4$, *Phys. Rev. B*, 2001, **63**, p 184108
10. Y.F. Shen, J. Tang, Z.H. Nie, Y.D. Wang, Y. Ren, and L. Zuo, Preparation and Application of Magnetic Fe_3O_4 Nanoparticles for Wastewater Purification, *Sep. Purif. Technol.*, 2009, **68**, p 312–319
11. S. Neveu, A. Bee, M. Robineau, and D. Talbot, Size-Selective Chemical Synthesis of Tartrate Stabilized Cobalt Ferrite Ionic Magnetic Fluid, *J. Colloid Interface Sci.*, 2002, **255**, p 293–298
12. C. Boyer, M.R. Whittaker, V. Bulmus, J. Liu, and T.P. Davis, The Design and Utility of Polymer-Stabilized Iron-Oxide Nanoparticles for Nanomedicine Applications, *NPG Asia Mater.*, 2010, **2**, p 23–30
13. A.O.G. Maia, C.T. Meneses, A.S. Menezes, W.H. Flores, D.M.A. Melo, and J.M. Sasaki, Synthesis and X-Ray Structural Characterization of NiO Nanoparticles Obtained Through Gelatin, *J. Non-Cryst. Solids*, 2006, **352**, p 3729–3733
14. H.M. Rietveld, Line Profiles of Neutron Powder-Diffraction Peaks for Structure Refinement, *Acta Crystallogr.*, 1967, **22**, p 151–152
15. R.A. Young, A. Sakthivel, T.S. Moss, and C.O. Paiva-Santos, DBWS-9411: An Upgrade of the DBWS Programs for Rietveld Refinement with PC and Mainframe Computers, *J. Appl. Crystallogr.*, 1995, **28**, p 366–367
16. G. Caglioti, A. Paoletti, and F.P. Ricci, Choice of Collimator for a Crystal Spectrometer for Neutron Diffraction, *Nucl. Instrum. Methods*, 1958, **35**, p 223–228
17. G.K. Williamsom and W.H. Hall, X-Ray Line Broadening from Filed Aluminum and Wolfram, *Acta Metall.*, 1953, **1**, p 22
18. L.J. Zhao and Q. Jiang, Effects of Applied Magnetic Field and Pressures on the Magnetic Properties of Nanocrystalline $CoFe_2O_4$ Ferrite, *J. Magn. Magn. Mater.*, 2010, **322**, p 2485–2487
19. D.L. Zhao, X.W. Zeng, Q.S. Xia, and J.T. Tang, Preparation and Coercivity and Saturation Magnetization Dependence of Inductive Heating Property of Fe_3O_4 Nanoparticles in an Alternating Current Magnetic Field for Localized Hyperthermia, *J. Alloy. Compd.*, 2009, **469**, p 215–218
20. B.P. Rao, G.S.N. Rao, A.M. Kumar, K.H. Rao, Y.L.N. Murthy, S.M. Hong, C.-O. Kim, and C. Kim, Soft Chemical Synthesis and Characterization of $Ni_{0.65}Zn_{0.35}Fe_2O_4$ Nanoparticles, *J. Appl. Phys.*, 2007, **101**, p 123902-1–123902-4
21. Z. Wang, B. Shen, Z. Aihua, and N. He, Synthesis of Pd/Fe_3O_4 Nanoparticle-Based Catalyst for the Cross-Coupling of Acrylic Acid with Iodobenzene, *Chem. Eng. J.*, 2005, **113**, p 27–34
22. A.C.H. Barreto, V.R. Santiago, S.E. Mazzetto, J.C. Denardin, R. Lavín, G. Mele, M.E.N.P. Ribeiro, I.G.P. Vieira, T. Gonçalves, N.M.P.S. Ricardo, and P.B.A. Fechine, Magnetic Nanoparticles for a New Drug Delivery System to Control Quercetin Releasing for Cancer Chemotherapy, *J. Nanopart. Res.*, 2011, **13**, p 6545–6553
23. A.C.H. Barreto, F.J.N. Maia, V.R. Santiago, V.G.P. Ribeiro, J.C. Denardin, G. Mele, L. Carbone, D. Lomonaco, S.E. Mazzetto, and P.B.A. Fechine, Novel Ferrofluids Coated with a Renewable Material Obtained from Cashew Nut Shell Liquid, *Microfluid. Nanofluid.*, 2012, **12**, p 677–686
24. Y.I. Kim, D. Kim, and C.S. Lee, Synthesis and Characterization of $CoFe_2O_4$ Magnetic Nanoparticles Prepared by Temperature-Controlled Coprecipitation Method, *Phys. B*, 2003, **337**, p 42–51
25. A. Ahlawat, V.G. Sathe, V.R. Reddy, and A. Gupta, Mossbauer, Raman and X-Ray Diffraction Studies of Superparamagnetic $NiFe_2O_4$ Nanoparticles Prepared by Sol-Gel Auto-Combustion Method, *J. Magn. Magn. Mater.*, 2011, **323**, p 2049–2054
26. S. Krehula and S. Musić, Influence of Cobalt Ions on the Precipitation of Goethite in Highly Alkaline Media, *Clay Miner.*, 2008, **43**, p 95–105
27. D.P.E. Dickson and F.J. Berry, *Mössbauer Spectroscopy*, Cambridge University Press, Cambridge, MA, 1986
28. A.S. Albuquerque, J.D. Ardisson, W.A.A. Macedo, J.L. López, R. Paniago, and A.I.C. Persiano, Structure and Magnetic Properties of Nanostructured Ni-Ferrite, *J. Magn. Magn. Mater.*, 2001, **226–230**, p 1379–1381
29. D.R. Patil and B.K. Chougule, Effect of Copper Substitution on Electrical and Magnetic Properties of $NiFe_2O_4$ Ferrite, *Mater. Chem. Phys.*, 2009, **117**(2009), p 35–40